Title: **Fumaric acid fermentation with immobilised *Rhizopus oryzae*: quantifying time-dependent variations in catabolic flux**

Authors: Andre Naude

Willie Nicol

Affiliation: Department of Chemical Engineering, University of Pretoria, Lynnwood Road, Hatfield, 0002, Pretoria, South Africa

Corresponding author: Willie Nicol

Tel.: +27124203796; Fax: +27124205048

E-mail: willie.nicol@up.ac.za; willie.nicol@gmail.com

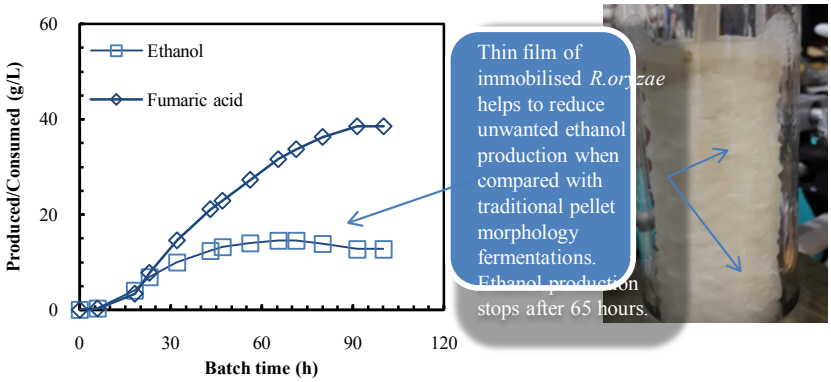

Graphical abstract

Highlights

- Three distinct production phases were observed.
- ATP production from respiration had an upper bound−2 mmol ATP.g biomass^{-1}.h^{-1}.
- Instantaneous fumarate yield highest when ethanol flux terminates.
- Higher DO and pH mitigated fumarate flux inhibition after ethanol flux termination.

Abstract

A novel fermenter system utilising immobilised *Rhizopus oryzae* is presented. The impact of dissolved oxygen (20%, 60% and 80%) and pH (4 and 5) was investigated. All fermentations exhibited three distinct phases. Phase A, at the start, was associated with no fumarate production, minimal respiration and ethanol as the major product. Phase B was characterised by the onset of fumarate production and significant ethanol and respiration fluxes. Phase C was associated with zero ethanol flux. Inhibition of fumarate production was more severe at low pH. The DO 20% fermentation (pH 5) had a low respiration flux which resulted in excessive ethanol production. Higher DO levels resulted in less inhibition of fumarate production during phase C. Instantaneous fumarate yields on glucose were at a maximum at the start of phase C, with values in excess of 0.75 $g.g^{-1}$ achieved for the DO 60% and 80% fermentations.

Keywords

Fumaric acid; Fermentation; Immobilization; Bioreactors; *Rhizopus oryzae*

Nomenclature

DO	dissolved oxygen concentration (% saturation)
EMP	Embden-Meyerhof-Parnas glycolysis pathway
FA	fumaric acid
HPLC	High Performance Liquid Chromatography
r_{ATP}^{E}	instantaneous ATP production rate by the ethanol pathway (mmol.g biomass^{-1}.h^{-1})
r_{ATP}^{R}	instantaneous ATP production rate by respiration (mmol.g biomass^{-1}.h^{-1})
r_{G}^{E}	glucose consumption rate towards ethanol production (g.g biomass^{-1}.h^{-1})
r_{G}^{F}	glucose consumption rate towards fumaric acid production (g.g biomass^{-1}.h^{-1})
r_{G}^{R}	glucose consumption rate towards respiration (g.g biomass^{-1}.h^{-1})
r_{G}^{T}	total glucose consumption rate
v_{G}^{E}	glucose flux towards ethanol production
v_{G}^{F}	glucose flux towards fumaric acid production
v_{G}^{R}	glucose flux towards respiration
Y_{GF}^{inst}	instantaneous fumaric acid yield on glucose (g.g^{-1})
Y_{GF}^{accum}	accumulative fumaric acid yield on glucose (g.g^{-1})

1. Introduction

Fumaric acid (FA) is one of the three, four-carbon dicarboxylic acids from the tricarboxylic acid (TCA) cycle. All three of these acids (malic, succinic and fumaric acid) have been identified by the USA Department of Energy as top value-added chemicals that can be derived from biomass with the potential of future bulk scale application [1]. Although succinic acid has received more attention in the open literature during the past two decades [2], fumaric acid has the advantage of a double bond that can be used for cross-linking in polymerisation [1]. This opens up the option of partially replacing the 2.1 Mton per annum maleic anhydride market [3], since unsaturated polyester resins derived from fumaric acid are reported to be non-toxic with greater polymer hardness when compared with resins derived from maleic anhydride [4]. Fumaric acid, in its undissociated form, has a lower water solubility than most organic acids which simplifies its purification and accordingly adds to the favourability of this bio-based chemical.

With the prospect of a growing bulk chemical market based on renewable feedstocks, optimisation of the fermentation process will become more important. *Rhizopus oryzae* (ATCC 20344) has established itself as the dominant microbial fumaric acid producer over the past decade in open literature research [4–6], while attempts at fumaric acid production with genetically modified microbial strains have failed to compete with *R. oryzae* [7,8]. Fermentation with *R. oryzae* typically entails the separate aerobic growth of the fungus, followed by an aerobic, non-growth production stage induced by nitrogen or phosphate limitation [9–12]. Fumarate is predominantly formed during the production stage with ethanol as the main by-product. Accordingly, *R. oryzae* has been viewed as a facultative anaerobe since it is capable of anaerobic fermentation [9], while ethanol produced during aerobic fermentation is typically attributed to oxygen diffusion limitations within the filamentous biomass [9,12] As a result, numerous fermentation studies target the formation of very small fungal pellets to limit carbon loss due to ethanol production [9,12,13]. This said, the elimination of ethanol formation has not yet been reported, despite extensive efforts [14].

The majority of *R. oryzae* fermentations employ mycelial pellets prepared in high-shear shake-flask fermentations [9,11,12,15]. Upscaling of pellet preparation remains a challenge since larger stirred vessels fail to create the high shear conditions required. Continuous operation with pellets also poses a major challenge since pellet separation from the outlet stream can easily result in severe clogging. Immobilisation successfully addresses both of these challenges as upscaling merely entails increasing the immobilisation support area, while biomass retainment via immobilisation side-steps the *in situ* pellet separation challenge for continuous operation. Accordingly, fungal immobilisation should be considered as an alternative for studying production physiology where continuous fermentations are typically used. In addition, immobilisation should also be considered in process scale-up as a means for controlling the fungal morphology.

Most *R. oryzae* fermentation studies focus on the final fumarate yield, titre and the average volumetric productivity to achieve the final conditions in a batch fermenter. Literature reviews therefore use these performance indicators for comparison [4,5]. The final state of the fermentation broth and the time taken to achieve this state are crucial parameters when considering further process development, yet these parameters provide little information on the physiology of the organism and how it changes with altering conditions. Proper understanding and quantification of the physiology will assist in future process designs where broth concentrations can be controlled either by steady state continuous operation or via *in situ* removal/addition of metabolites. Industrial fermentation can only move beyond the domain of batch processes if there is proper metabolic understanding of the microbial producer.

Fermentation with *R. oryzae* (ATCC 20344) is characterised by three main carbon flux branches, namely fumarate production, ethanol production and aerobic respiration [5] (see detailed pathway map in Fig. 1). Although the fumarate production pathway shares a section of the TCA cycle with the respiration pathway, these pathways will be separated since respiration occurs within the mitochondria (oxidative TCA cycle), while the reductive (reverse) TCA cycle,

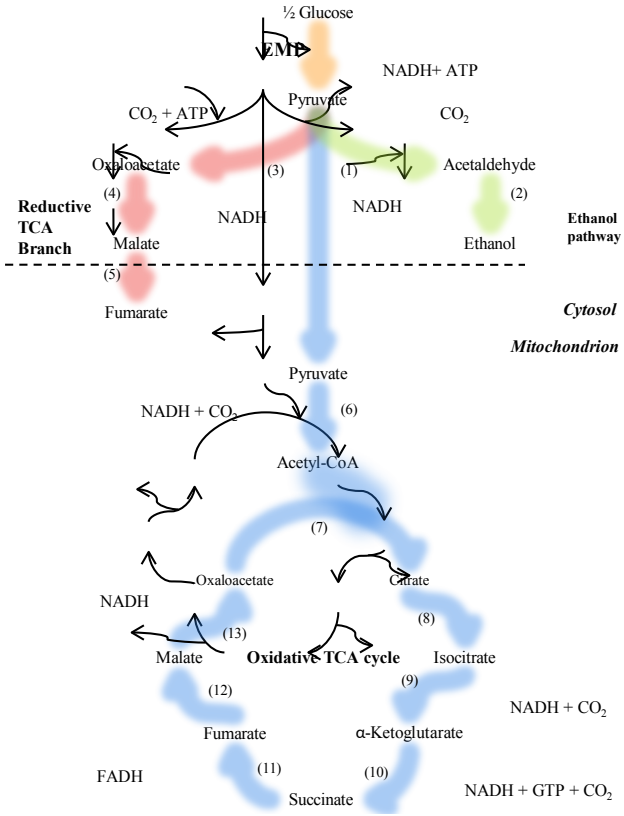
½ Glucose
EMP
NADH+ ATP
Pyruvate
CO_2 + ATP
CO_2
Oxaloacetate
(3)
(1)
Acetaldehyde
(4)
(2)
Reductive TCA Branch
NADH
NADH
Ethanol pathway
Malate
Ethanol
(5)
Fumarate
Cytosol
Mitochondrion
Pyruvate
NADH + CO_2
(6)
Acetyl-CoA
(7)
Oxaloacetate
Citrate
NADH
(8)
(13)
Malate
Oxidative TCA cycle
Isocitrate
(9)
(12)
NADH + CO_2
Fumarate
α-Ketoglutarate
FADH
(11)
(10)
NADH + GTP + CO_2
Succinate

Fig. 1 Metabolic pathways for *Rhizopus oryzae* (ATCC 20344). Enzymes are indicated by bracketed numbers: 1 Pyruvate decarboxylase, 2 Alcohol dehydrogenase, 3 Pyruvate carboxylase, 4 Malate dehydrogenase, 5 Fumarase, 6 Pyruvate dehydrogenase complex, 7 Citrate synthase, 8 Aconitase, 9 Isocitrate dehydrogenase, 10 α-Ketoglutarate dehydrogenase and Succinyl-CoA synthase, 11 Succinic dehydrogenase, 12 Fumarase, 13 Malate dehydrogenase

which is responsible for fumarate accumulation, occurs in the cytosol [16]. Quantification of the carbon flux distribution between these three main pathways is essential for developing a competitive process.

In this study, a novel fermenter was developed whereby *R. oryzae* was immobilised on both sides of a polypropylene pipe. The initial glucose concentration of the growth stage was used to control the morphology of the attached biomass whereby a homogeneous fungal matt of desired thickness was established. Although the long-term goal is to use the fermenter system for continuous operation, the initial objective (presented in this study) was to study the effect of pH and dissolved oxygen concentration (DO) on the unique biomass morphology employed. Batch fermentations were used to characterise the time-dependent catabolic flux variations. The pH was varied between 4 and 5 and the DO was controlled at 20%, 60% and 80% saturation. The off-gas from batch fermentations of immobilised *R. oryzae* was analysed for oxygen and carbon dioxide in addition to the standard liquid measurements. This resulted in an over specified dataset which was reconciled with a mass balance before calculations were performed. Emphasis was placed on changes in the instantaneous metabolic flux characteristics of the organism. The idea was to identify target conditions with high fumarate yield and rate of production.

2. Materials and methods

2.1 Microorganism and culture conditions

R. oryzae (ATCC 20344*)* was obtained from the Spanish collection of cultures (Colección Española de Cultivos Tipo, Valencia, Spain). The cultures were grown at 35 °C on potato dextrose agar plates (Merck, South Africa) for 96 hours to produce spores. After growth, the plates were washed with distilled water and filtered through sterile filter paper to create a spore solution. Spore solutions were checked for purity and viability by inoculating a part of the solution into 200 mL of sterilised tryptone soy broth (Merck, South Africa). After incubation for

48 hours at 35 °C, High Performance Liquid Chromatography (HPLC) analysis was used to determine whether the spore solutions were pure and viable by checking for unknown metabolites.

2.2 Medium

The growth medium consisted of (in units of $g.L^{-1}$): 5 glucose, 2 urea, 0.6 KH_2PO_4, 0.25 $MgSO_4.7H_2O$ and 0.088 $ZnSO_4.7H_2O$. The fermentation medium consisted of (in units of $g.L^{-1}$): 100 glucose, 0.6 KH_2PO_4, 0.25 $MgSO_4$, 0.088 $ZnSO_4.7H_2O$ and 1 yeast extract. All media components were obtained from Merck (South Africa). Distilled water was used and all media were sterilised in an autoclave at 121 °C for 60 minutes. The glucose and urea were sterilised separately from the rest of the components.

2.3 Fermentation

The novel reactor, illustrated in Fig. 2, consisted of a glass cylinder with an outer diameter of 50 mm contained between an aluminium base and head. The working volume of the reactor was 220 mL. A polypropylene pipe with an outer diameter of 34 mm and a length of 170 mm was used as attachment surface for the fungus; attachment occurred on both sides of the pipe. An external recycle line from the head to the base of the reactor was used for agitation. This resulted in enhanced shear over the surface of the pipe compared with traditional agitation methods, which led to improved oxygen transfer. The recycle pump (120 $mL.min^{-1}$) switched direction every 30 seconds to ensure that there was no accumulation of biomass in the recycle line; this also improved mixing within the reactor. All reservoir vents, gas inlets and outlets used 0.2 µm PTFE membrane filters (Midisart 2000, Sartorius, Germany) to prevent contamination. Temperature was controlled at 35 °C by the hotplate on which the fermenter rested. The temperature measurement was taken via a thermocouple housed within an aluminium sheath positioned in the recycle line. The pH was measured using a CPS 71D glass pH probe (Endress & Hauser, Germany) housed within an aluminium probe holder situated in

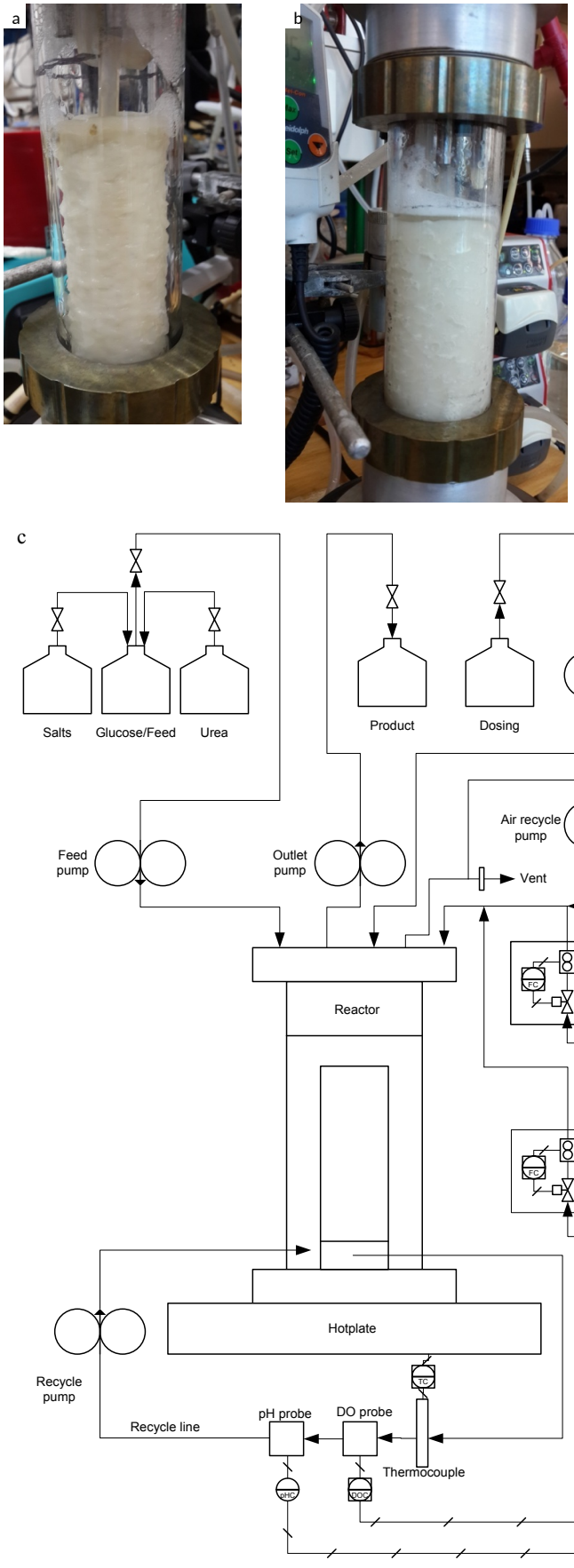

Fig. 2. Images of the fermenter at the end of the growth stage (a) and during the production stage (b) with the fermenter setup (c) below.f

the recycle line. The pH probe was connected to a Liquiline CM442 transmitter (Endress & Hauser, Germany) which controlled the dosing of 3M NaOH.

Instrument-grade air (Afrox, South Africa), a dry mixture of synthetic air (20% O_2 and 80% N_2), was sparged through the reactor. Air flow into the reactor was controlled at 22 mL.min^{-1} (10% vvm) using an SLA5850 (Brooks, USA) mass flow controller. The dissolved oxygen (DO) level was measured using a COS 22D probe (Endress & Hauser, Germany) housed within an aluminium probe holder situated in the recycle line. The DO probe was connected to a Liquiline CM442 transmitter and the DO was controlled by switching an air recycle pump. This pump recycled air exiting the top of the reactor back into the sparger at a flow rate of 660 ml.min^{-1} (3 vvm).

2.4 Morphology control

The primary goal during the growth phase is to develop a thin biofilm which is evenly spread over the surface of the polypropylene pipe. Initial glucose and spore concentration were found to be the governing parameters. Small inoculum volumes resulted in initial spore concentrations below 10^5 spores per litre of fermenter and caused sporadic areas of growth regardless of the initial glucose concentration. Initial fermenter spore concentrations equal to or greater than 10^5 spores per litre ensured even biofilm growth. The initial glucose concentration determined the thickness of the biofilm, with higher concentrations resulting in a thicker biofilm. Very low initial glucose concentrations (< 2.5 g/L) resulted in sporadic biofilm growth, regardless of the inoculum size. An initial glucose concentration of 5 g/L was used. This resulted in a biofilm thickness of 1 mm. The pH and DO were controlled at 5 and 60% respectively during the growth phase. Identical conditions were used for all growth phases. The switch to the production phase was made after O_2 consumption/CO_2 production started to slow during the growth phase. Fig. 2 shows the fermenter during the growth and production stages.

2.5 Analytical methods

HPLC was used to determine the glucose, fumaric acid, ethanol, malic acid, glycerol and succinic acid concentrations in the broth. Analyses were performed using an Agilent 1260 Infinity HPLC (Agilent Technologies, USA) equipped with a refractive index (RI) detector (55 °C) and a 300 mm x 7.8 mm Aminex HPX-87H ion-exchange column (Bio-Rad Laboratories, USA). The mobile phase (0.3 $mL.L^{-1}$ H_2SO_4) flow rate was 0.6 $mL.min^{-1}$ with a column temperature of 60 °C. Outlet gas composition (CO_2 and O_2) was measured using a Tandem gas analyser (Magellan Biotech, UK). The air was dried before it entered the gas analyser in order to remove the influence of ethanol and water vapour on the gas measurement. Biomass was filtered on pre-weighed filter paper (47 mm, Whatman, Sigma Aldrich, South Africa) and washed with distilled water. The biomass was left to dry at 90 °C for 24 hours and weighed to yield the final amount of dry biomass.

2.6 Data reconciliation

This study had nine variables in total during the production stage: glucose, ethanol, fumaric acid, malic acid, glycerol, succinic acid, CO_2, O_2 and water. Excluding water, all of the abovementioned variables were measured which equates to eight measured variables. The nine variables are connected through three component balances: carbon, hydrogen and oxygen. The eight measured variables and three component balances cause this system to be overspecified by two measurements. This overspecification can be used to quantify gross measurement errors through data reconciliation [17]. The data reconciliation method by Wang and Stephanopoulos [18] was used in this study; this method is also summarised by Villadsen et al. [17]. It requires an estimation of the expected size of the errors for each of the measured variables. Excluding ethanol, all measurements from HPLC samples (in units of $cmol.L^{-1}$) are expected to have an error of ±0.003 + 2% of the measured concentration. For ethanol the error is expected to be ±0.003 + 7% of the measured concentration; the increased error size is due to the evaporation of ethanol. The error for the gas measurements is expected to be ±10% of the total amount measured due to measurements falling within the lower section of the measurement range of the

gas analyser. The expected errors were all independent of one another. Appendix A explains the data reconciliation method in greater detail.

3. Results and discussion

3.1 Growth phase

Growth profiles are given in Fig. 3. The mass of immobilised biomass was inferred from the mass balance. Note that data reconciliation was not used for growth given that there is only a single overspecification. Apart from CO_2, ethanol was the only significant catabolite formed during growth. A standard Monod model was used to describe the growth (Equation 1), note that the *Ks* value was estimated to be very low and given the range of the glucose concentration during growth (from 5 g/L to 0.5 g/L) it was discarded in Equation 1 as shown. The yields, given by the slope in Fig. 3, remained constant throughout the growth stage, with the yield values given in Table 1. The switch was made between the growth phase and the production phase when the rate of CO_2 production/O_2 consumption (respiration) started to decline. This was indicated by the online DO and gas composition measurements. The glucose concentration in the growth medium is at 0.5 g/L once respiration begins to decline. Therefore, there is a small time window (< 20 minutes) wherein the switch had to be made in order to prevent any damage to the fungi due to substrate exhaustion.

The switch was performed by pumping the growth medium out of the reactor with the pump in Fig. 2 and refilling the reactor with the fermentation medium. In order to increase the mass balance accuracy and to insure that there was no accidental carryover from the growth medium, the fermentation medium was drained and refilled with another batch of fresh fermentation medium after 5 minutes of mixing.

$$\mu = \mu_{max} \frac{S}{K_s + S} \qquad (1)$$

Table 1. Parameters fitted during the growth phase

Parameter	Value
u_{max}(h)	0.35
Y_{XS} (g.g)	2.307
Y_{SE} (g.g)	0.160
Y_{SC} (g.g)	0.381
Y_{SO} (g.g)	0.138

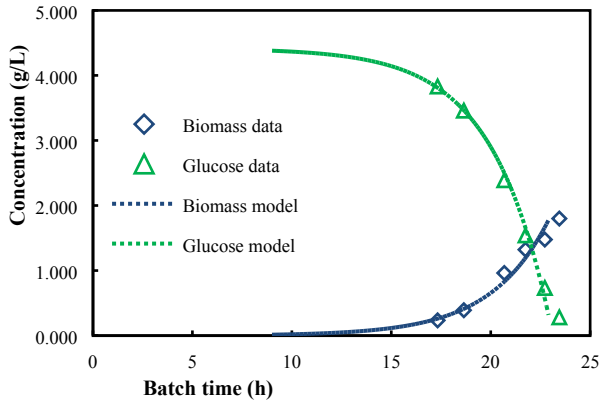

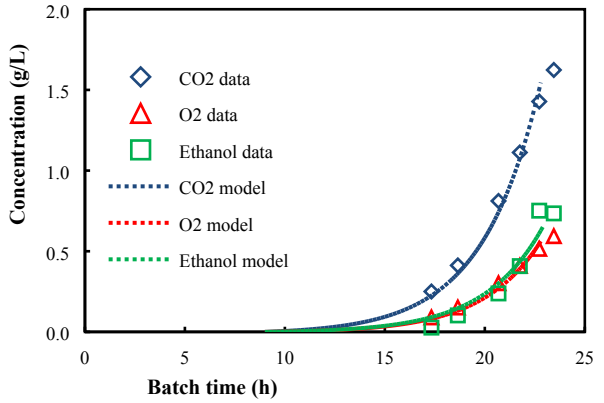

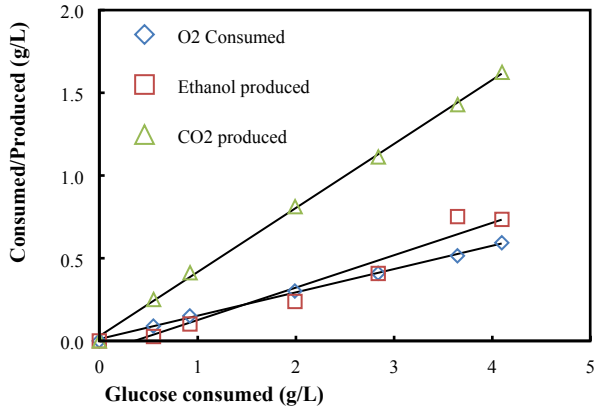

Fig. 3. Data from the growth phase of the fermentation.

$$\mu = \mu_{max}$$

3.2 Reconciled production results (zero growth)

Only reconciled data are used for figures and tables. The raw HPLC and off-gas measurements are given as part of the supplementary material (Appendix B). The main deviations between raw and reconciled data were on glucose consumed and ethanol produced. Reconciled glucose consumption rates were lower than the raw counterparts for all runs. The average reconciled glucose consumption value was 10% lower than that of the raw measurement. This difference was attributed to an incorrect estimation of the base dilution effect during the batch run, where more base was added than estimated. Reconciled ethanol production was higher than that of the raw counterpart, especially in the later stages of the fermentation during which a significant amount of ethanol was present in the broth. The same trend was observed for all the runs, with reconciled ethanol amounts being up to 20% higher than the raw values. These differences were attributed to ethanol evaporation and agree with the findings of Rao Engel et al.[12], who found that significant ethanol losses were detected when ethanol concentrations exceeded 5 $g.L^{-1}$.

A repeat fermentation was performed at the pH 5, DO 60% condition. The profiles were similar in shape, but a distinct difference in lag phase duration (adaptation period when switching media) was observed between the repeat fermentations. A five-hour shift to align the data resulted in an overlap of consolidated measurements that were within a 5% deviation band. This indicates repeatability in the profile shape but variation with regard to the adaptation period when switching from the growth medium to the production medium. Accordingly, the results should be interpreted by examining the entire production phase rather than the absolute time of the fermentation. The differences in the total amount of biomass between repeat experiments were less than 5%.

The four separate fermentation runs are plotted in Fig.4. The DO and pH are compared separately in these figures. Minor by-products like glycerol, succinic and malic acid are given in

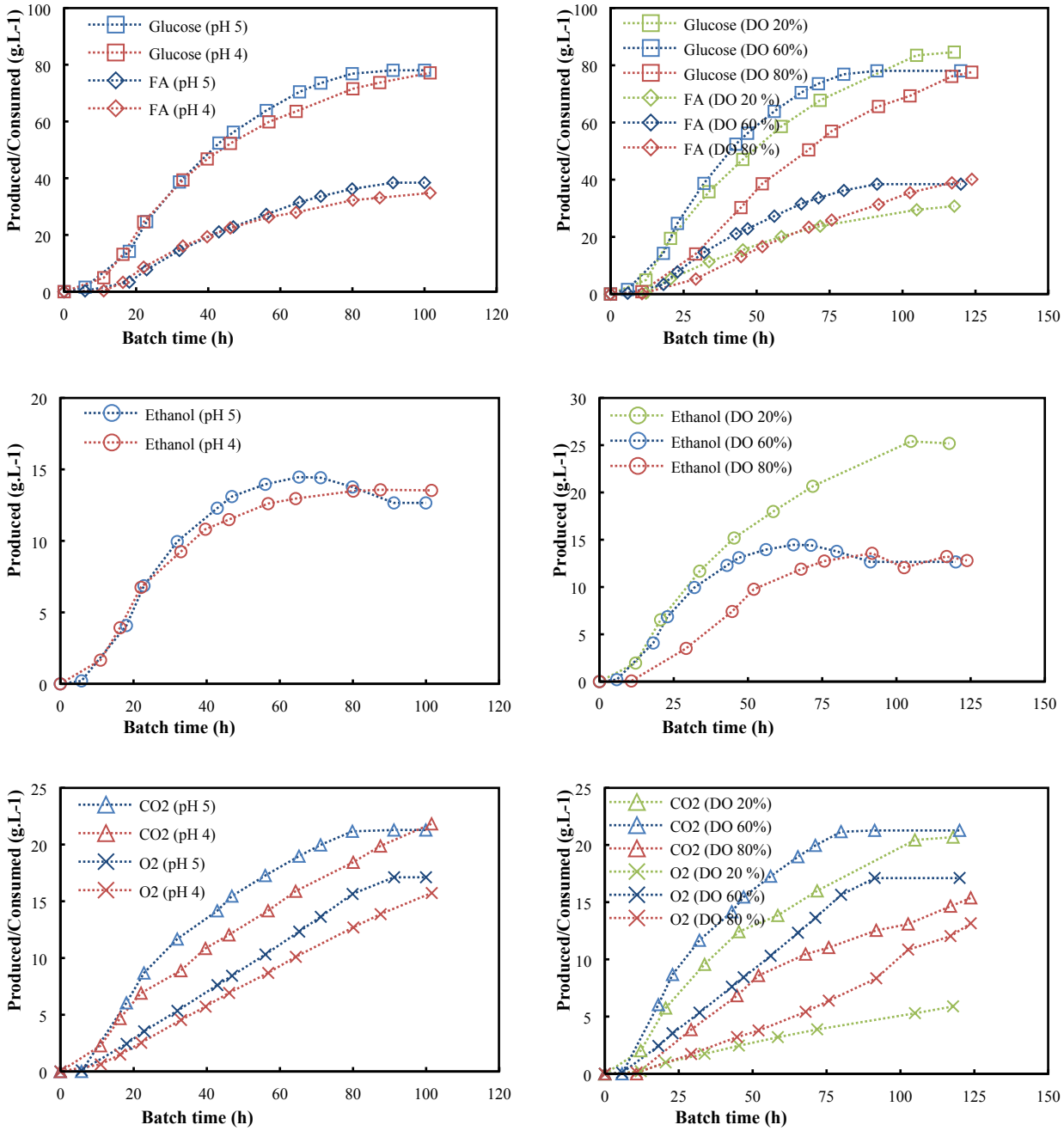

Fig. 4. Reconciled fermentation profiles at different pH and DO values. Concentrations are based on the actual mass produced/consumed divided by the initial (t=0) fermenter volume.

the supplementary dataset (Appendix B). These products account for less than 8% of glucose consumed at all times and are not discussed in detail. The concentrations given in Fig. 4 are based on the mass of component in the fermenter divided by the initial fermenter volume. The fermenter volume fluctuated slightly during fermentation due to base dosing and sample removal and this was incorporated into the mass calculations.

All fermentation runs exhibited three distinct phases of production. Phases were separated by using the onset of fumarate production and the termination of ethanol production as boundaries. Accordingly, phase A (at the start) is characterized by zero fumarate production, phase B by fumarate and ethanol production and phase C (at the end) by fumarate production with zero ethanol production. Phase A typically lasted less than 20 hours and most of the glucose is converted to ethanol, although a limited amount of respiration does occur as can be seen from the oxygen consumption profiles in Fig. 4. Whilst it has been assumed that the onset of fumarate production is caused by a nutrient limitation (nitrogen) [5], initial experiments have shown that the length of phase A can be shortened by the addition of nitrogen in low concentrations. Similar results have been shown in other studies where the initial C:N ratio was varied in the production phase [19]. Phase B is characterised by fumarate and ethanol formation with a significant amount of respiration. Phase B lasted between 40 and 100 hours depending on the external conditions. Phase C can be identified by the tapering of the ethanol profile with continued fumarate production and is also associated with significant respiration. From a fumarate yield viewpoint, production in phase C should be targeted where wastage to ethanol does not occur. The trade off in the phase is the declining fumarate productivity and care should be taken in maintaining a sufficient production rate.

A comparison of the overall performance for the four different fermentation runs is given in Table 2. These results are based on the broth concentration when all the glucose is consumed. The results can be directly compared to other fumaric acid fermentations where the conventional pellet morphology was used. When considering the influence of DO on the overall

Table 2 Experimental data at the end of each fermentation at different pH and DO values

Fermentation	1	2	3	4
pH	4	5	5	5
DO	60%	60%	80%	20%
Biomass (g)	1.76	1.88	1.63	1.49
FA titre ($g.L^{-1}$)	34.81	38.43	40.13	30.74
Average FA productivity ($g.g\ biomass^{-1}.h^{-1}$)	0.043	0.049	0.044	0.039
Average FA productivity ($g.L^{-1}.h^{-1}$)	0.34	0.42	0.32	0.26
FA yield ($g.g^{-1}$)	0.45	0.49	0.52	0.36
Ethanol yield ($g.g^{-1}$)	0.18	0.16	0.17	0.30

fermentation outcome it is clear that the DO 20% run resulted in poor fumarate yields due to excessive ethanol production. The fumaric acid yield of 0.36 $g.g^{-1}$ is similar to those in pellet morphology studies where very large pellets (> 2 mm) were used [13]. Most pellet morphology studies claim that oxygen diffusion limitations in large pellets are responsible for ethanol production [12,13] which explains the similar results with the DO 20% fermentation. When the DO is increased to 60% the fumarate yield improves significantly (0.49 $g.g^{-1}$). These results are similar those obtained by Fu et al. [20] (0.51 $g.g^{-1}$ using 0.2 mm pellets) and Zhou et al. [13] (0.45 $g.g^{-1}$ using 0.5 mm pellets) and significantly higher than those by Roa Engel et al. [12] (0.31 $g.g^{-1}$ using 0.5 mm pellets). A further increase in the DO to 80% saturation resulted in slight yield increase (0.52 $g.g^{-1}$). Both the DO 60% and DO 80% fermentations exhibited phase C behaviour where zero ethanol was formed. This suggests that oxygen diffusion limitations are not the cause of ethanol production for the immobilised morphology when the DO is maintained at a sufficient level (> 60%). Phases with zero ethanol production have not been reported in pellet morphology fermentations.

Previous studies by Roa Engel et al. [12] (using the pellet morphology) show that the ideal pH during the production is between 4 and 5 with minimal variation between the two values. This is in agreement with the results from this study. With the regards to the effect of pH on growth, the pellet morphology was reported to be highly dependent on the initial pH and shaker speed [12,13]. In contrast, the immobilised morphology was found to be pH insensitive during the growth stage, where total biomass and matt thickness did not change with pH (3.5 – 7). This poses an advantage for the immobilised setup, especially with regards to scale up. Small pellets are usually prepared in shaking flasks smaller than 1L [12], in order to produce these pellets in a large scale the same shear conditions will have to be repeated in a larger vessel which will lead to higher equipment costs just to ensure the correct morphology.

These overall results are by definition accumulative and provide little insight into the metabolic flux variations that occurred during fermentations. The next section addresses this issue by scrutinising the instantaneous flux characteristics of the different phases.

3.2 Metabolic flux distribution

The flux model of the non-growth fermentation can be simplified by giving the overall pathways of the three main carbon fluxes. Neglecting the minor by-products (glycerol, succinic acid and malic acid) will result in the following three pathway equations with the stoichiometries based on a P:O value of 1.25 for the oxidative phosporylation steps as discussed by Villadsen et al. [17]:

$$v_G^F: C_6H_{12}O_6 + 2CO_2 \rightarrow 2C_4H_4O_4 + 2H_2O \quad (2)$$

$$v_G^E: C_6H_{12}O_6 \rightarrow 2C_2H_6O + 2CO_2 + 2ATP \quad (3)$$

$$v_G^R: C_6H_{12}O_6 + 6O_2 \rightarrow 6CO_2 + 6H_2O + 19ATP \quad (4)$$

The fumarate (v_G^F), ethanol (v_G^E) and respiration (v_G^R) fluxes combine in various ratios to result in the overall stoichiometry given by:

$$v_G^T: C_6H_{12}O_6 + Y_{GO}O_2 \rightarrow Y_{GF}C_4H_4O_4 + Y_{GE}C_2H_6O + Y_{GC}CO_2 + Y_{GW}H_2O + Y_{GA}ATP \quad (5)$$

The yield ratios (Y_{ii}) will vary depending on the flux distribution between v_G^F, v_G^E and v_G^R. The fitting of smooth polynomials on the reconciled batch profiles allows the determination of instantaneous production/consumption rates (r) of all the components in Equation 5 by calculating the value of the derivative at a specific point in time. The corresponding instantaneous yield values can be obtained by using the ratio of the rates. The flux distribution is best represented by breaking down the total glucose consumption rate (r_G^T) into its respective parts, where:

$$r_G^T = r_G^F + r_G^E + r_G^R \quad (6)$$

The effect of pH on the instantaneous flux distribution in phases B and C is represented in Fig. 5(a+b). The three separate glucose consumption rates (r_G^F, r_G^E and r_G^R) are stacked on top of one another to provide an indication of the total glucose consumption rate (r_G^T) and the relative contribution of the separate rates. The value of the separate rates can be obtained from the vertical thickness of the specific colour slab. The first notable observation in Fig. 5(a+b) is the severe decrease in r_G^T for both fermentations 1 and 2 as the time increased. It is also clear from these figures that that the value of r_G^R remains relatively constant over time for both fermentations. This suggests that respiration occurs at a constant rate where the aerobic rate of ATP generation is approximately 2 mmol ATP.g biomass^{-1}.h^{-1}, as indicated in Fig. 5(e+f). In contrast to respiration, r_G^E decreases with time up to a point where zero ethanol is formed (r_G^E=0). From Fig. 5(e+f) it can be seen that the total ATP generation rate (mmol ATP.g biomass^{-1}.h^{-1}) decreases over time as the ethanol component disappears. This can be interpreted as inactivation of the biomass, although the inactivation occurs only in the anaerobic or ethanol-producing 'part' of the biomass. Note the difference when compared with the growth phase (Fig. 3) where the fraction of glucose tends towards the ethanol and respiration pathways during the entire growth phase. This suggests that the ethanol decrease seen in Fig. 5 is not due to DO oxygen effects.

From Fig. 5(a+b) one observes a clear decline in r_G^F, especially after ethanol production ceases. Noteworthy is the difference between the magnitude of r_G^F for fermentations 1 and 2, especially at the end of the fermentation (phase C) when r_G^F is at its lowest. The inhibition of r_G^F is most likely caused by the fumarate concentration itself [21,22,19,23], with the effect being more severe at low pH conditions (fermentation 1). The instantaneous fumarate yields (Y_{GF}^{inst}) for fermentations 1 and 2 are given in Fig. 6(a). The initial increase in yield is linked to the decrease in the ethanol flux, whereas the later decrease in phase C is linked to the diminishing r_G^F

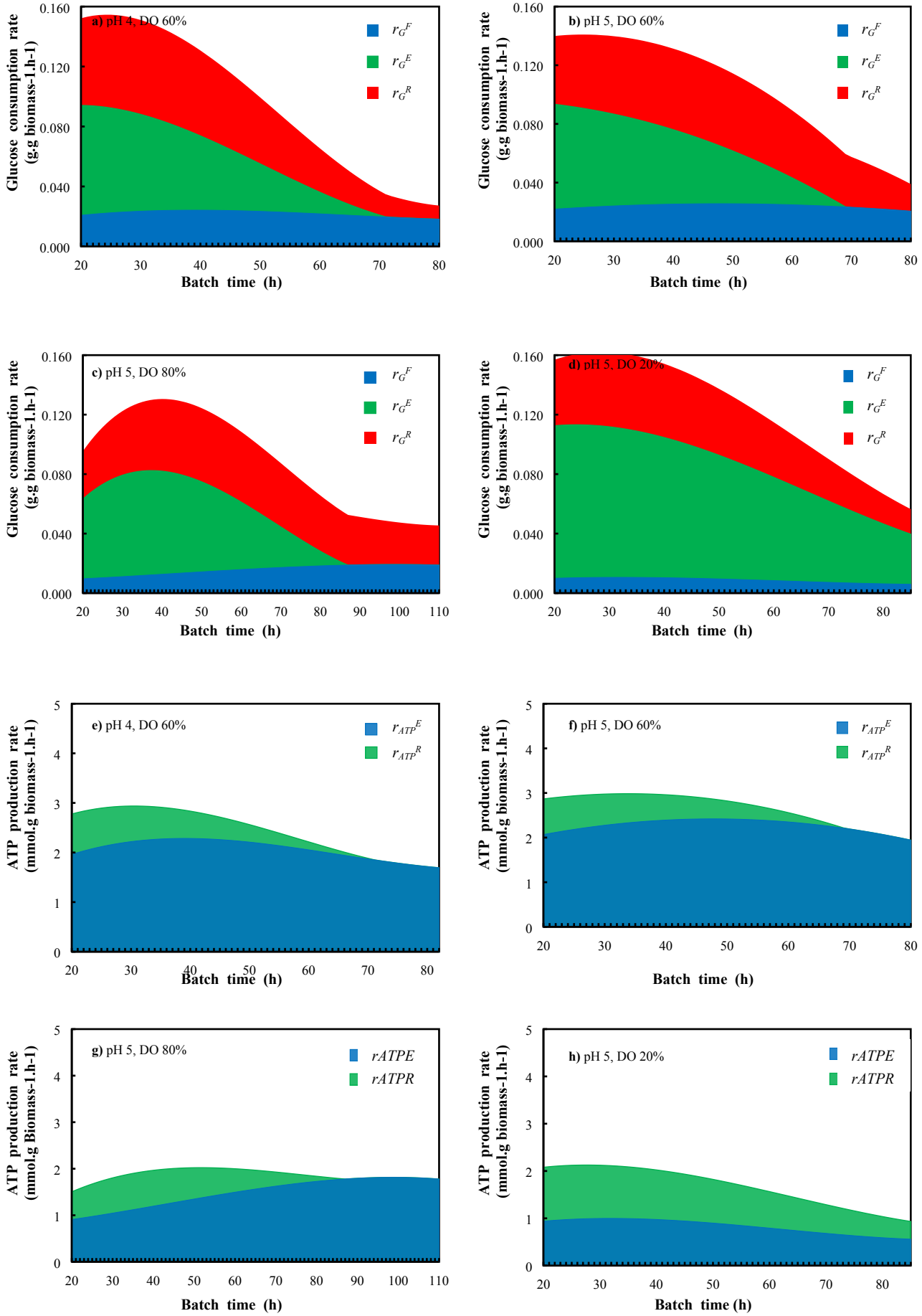

Fig. 5. Flux breakdown of the dynamic glucose consumption rate. The fluxes to fumarate (r_G^F), ethanol (r_G^E) and respiration (r_G^R) are shown as stacked slabs in graphs a–d. ATP formed from the ethanol pathway (r_{ATP}^E) and respiration (r_{ATP}^R) are shown as stacked slabs in graphs e–h. pH and DO levels are given at the top of each graph.

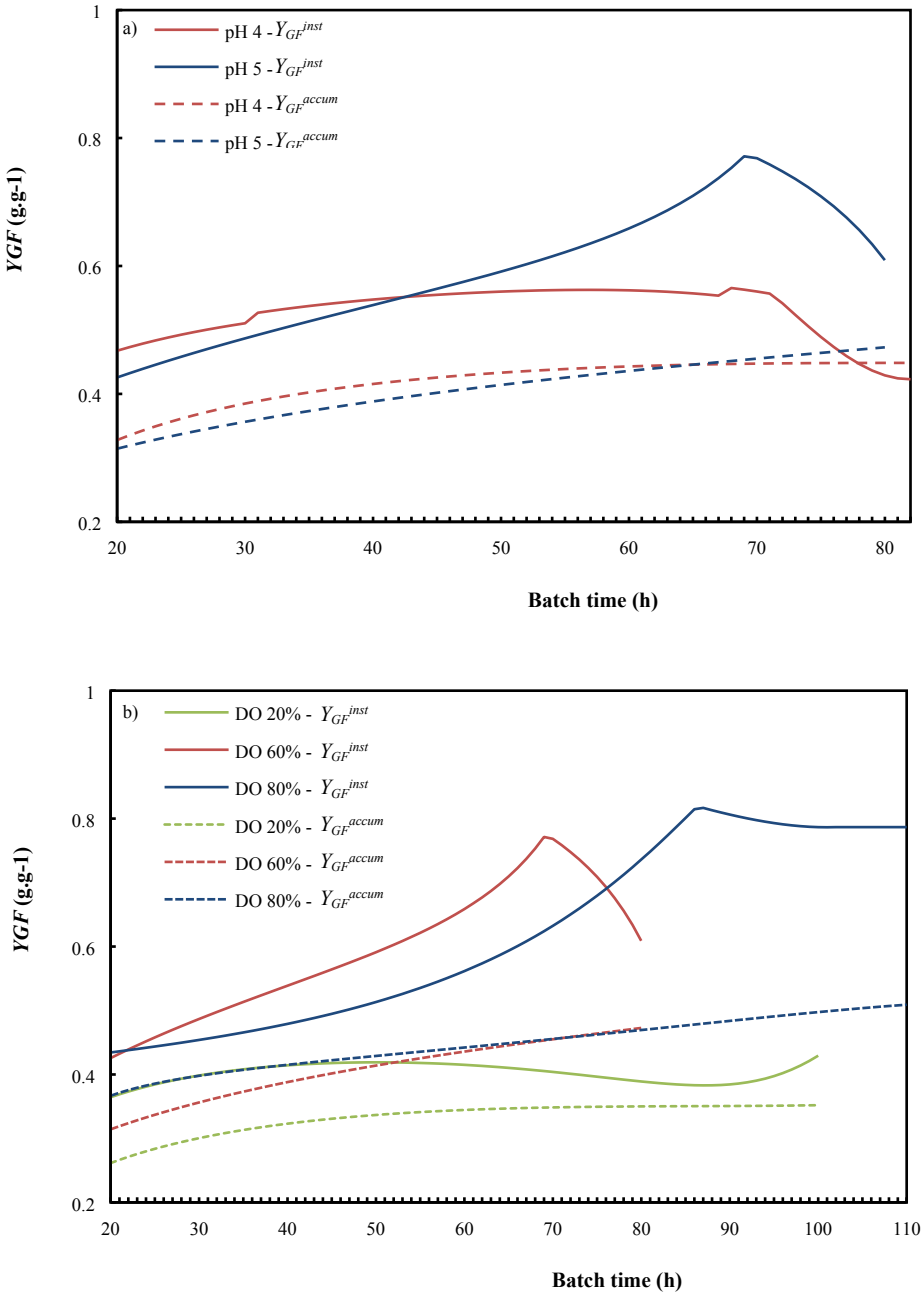

Fig. 6. Instantaneous and accumulative fumarate yield on glucose (Y_{GF}) for different pH (top) and DO (bottom) values.

relative to the constant respiration flux (r_G^R). It is interesting to note that fermentation 2 achieves a maximum Y_{GF}^{inst} of 0.77 g.g^{-1}. Fig. 6 also gives the accumulative yields (Y_{GF}^{accum}) as a function of time. The difference in Y_{GF}^{accum} between the two pH levels is not clear from these profiles due to the relatively small contribution of phase C production towards the overall yield. This can, however, be altered by prolonged operation in phase C, where fumarate production without ethanol production will contribute to the improved utilisation of carbon sugars.

The effect of DO on the flux distribution is given in Fig. 5(b−d). The first observation is that low DO concentrations (DO 20%) result in significantly higher ethanol production, while the respiration flux (r_G^R) is less than half of the value obtained in Fig. 5(a+b). This is in agreement with the behaviour of a facultative anaerobe under oxygen limitation, where additional energy (ATP) is generated via the anaerobic pathway towards ethanol. It can be seen from Fig. 5(h) that the total ATP generation rate at 20 hours was similar to the constant respiration value of Fig. 5(e+f). However, the argument of anaerobic compensation does not apply for the highly oxygenated run (DO 80%) during which r_G^R reached the same value as the DO 60% fermentations (1 and 2) when entering phase C. This implies that the oxygen consumption rate does not increase, despite a 33% higher oxygen concentration on the external surface of the biofilm. It appears that a respiration threshold or capacity exists, corresponding to an aerobic energy generation rate of approximately 2 mmol ATP.g biomass^{-1}.h^{-1}. This suggests that diffusion limitations within the biofilm are not limiting the oxygen consumption rate when the DO is above 60%. Nevertheless, a significant amount of ethanol was still produced for all the highly oxygenated cases (fermentations 1, 2 and 3). Accordingly, ethanol production cannot be attributed solely to regions of low or depleted DO within the biofilm as previously suggested [12]. A metabolic overflow mechanism is present that is unrelated to the oxygenation state within the biofilm.

When the DO 60% and 80% fermentations are compared, it is evident that the DO 80% case experienced a lag in phase B operation. Both the respiration and ethanol fluxes started slowly,

with r_G^E reaching higher values compared with the DO 60% case, most likely compensating for respiration not yet having achieved the capacity value in phase B. Similar cases of lag due to high DO levels have been reported in previous studies Fu et al. [14]. A difference can also be observed in phase C – here the fumarate flux for the DO 80% fermentation (r_G^F) remains relatively constant compared with the DO 60% fermentation, where a significant decrease was observed between 70 and 80 hours. This effect is clearly illustrated in Fig. 5(c), where the instantaneous fumarate yield profile (Y_{GF}^{inst}) for the DO 80% case plateaus around 0.8 $g.g^{-1}$ once phase C is reached. The effect can also be observed in the difference between the final accumulative yields of 0.49 vs 0.52 $g.g^{-1}$, for the DO 60% and 80% cases respectively. The overall difference might be small, but will become significant if prolonged operation in phase C is achieved. Higher DO values will therefore enhance the fumarate flux without altering the rate of oxygen consumption. Under these conditions high fumarate productivity can be maintained in the high yield phase (C) of production.

The metabolic flux results from the different batch runs should be used to develop new fermentation approaches in which high fumarate yield and productivity are targeted. The primary objective will be to operate within phase C in order to bypass substrate wastage to ethanol. It is uncertain whether phase C operation is caused by the concentration conditions in the broth or the time-dependent state of the organism. It has, however, been established that ethanol production is not permanently deactivated once phase C is achieved. Cao et al. [10] found that ethanol production was still present for all repeat batch cycles, even though phase C was reached at the end of all the cycles. The stability of the respiration flux in phase C reassures that prolonged operation within this phase is possible, i.e. the respiratory part of the biomass remains active and can fulfil the maintenance energy requirements. One approach to prolonging phase C operation is by increasing the substrate concentration in batch fermentations. Alternatively, continuous operation can be considered where stable (and favourable) concentration conditions can be maintained within the fermenter. This remains to be tested. The

secondary objective will be to increase the fumarate flux during phase C production. This can be visually interpreted as thickening the red slabs in Fig. 5(a–d). From the results of this study it is evident that higher pH and DO assist in mitigating the fumarate flux inhibition. Fumarate yields in excess of 0.8 g.g^{-1} will be possible if the fumarate flux (r_G^F) increases relative to the constant or capacity respiration flux (r_G^R). In short, it appears that operational changes can appreciably improve the profitability of the fermentation.

4. Conclusions

The results from the novel fermenter system indicated that conditions exist where zero ethanol is formed. This occurred at the end of the fermentation (phase C) where a decrease in fumarate production rate was observed, while the carbon utilised for respiration remained constant. Higher pH and DO levels resulted in a less inhibited fumarate flux in phase C, whereby the instantaneous fumarate yield increased. The biomass exhibited a maximum respiration capacity above a DO of 60%, suggesting that ethanol production is not solely linked to anaerobic zones within the biomass as previously suggested.

Acknowledgement

The financial assistance of the National Research Foundation (NRF) of South Africa towards this research is hereby acknowledged.

Appendix A

This section explains the data reconciliation method (Section 2.5) in more detail. The fluxes used in the data reconciliation discussion are numbered as follows (in units of cmol.L^{-1}): glucose (V_1), fumaric acid (V_2), ethanol (V_3), malic acid (V_4), glycerol (V_5), succinic acid (V_6), CO_2 (V_7), O_2 (V_8) and H_2O (V_9). The three elemental balances (carbon, hydrogen and oxygen) are given by Equations A-1, A-2 and A-3 respectively.

$$-V_1 + V_2 + V_3 + V_4 + V_5 + V_6 + V_7 = 0 \quad \text{(A-1)}$$

$$-2V_1 + V_2 + 3V_3 + \frac{6}{4}V_4 + \frac{8}{3}V_5 + \frac{6}{4}V_6 + 2V_9 = 0 \quad \text{(A-2)}$$

$$-V_1 + V_2 + 0.5\,V_3 + \frac{5}{4}V_4 + V_5 + V_6 + 2V_7 - 2V_8 + V_9 = 0 \quad \text{(A-3)}$$

As discussed in Section 2.5, there are nine variables in total, with eight of them being measured (V_1 to V_8). The three equations (A1−A3) imply that the system is overspecified by two and therefore data reconciliation can be used to identify gross measurement errors. The data reconciliation procedure by Villadsen et al. [17] was used and will be explained by means of an example. In this example the final data point (91 hours fermentation time) from the pH 5, DO 60% fermentation (Table B-1) will be reconciled to determine the corresponding value in Table 3.

The first step is to determine the coefficient matrices for the measured variables ($\mathbf{E_m}$) and for the calculated variables ($\mathbf{E_c}$). The three component balances (Equations A1−A3) are used to determine the coefficient matrices. In $\mathbf{E_m}$ and $\mathbf{E_C}$ every row corresponds to one of the component balances (Equations A1−A3). Therefore row one corresponds to the carbon balance, row two to the hydrogen balance and row three to the oxygen balance. Each column corresponds to one of the nine variables; $\mathbf{E_m}$ has eight columns which correspond to the coefficients of V_1−V_8 in the component balances, while $\mathbf{E_c}$ only has one column which

corresponds to the coefficients of V_9 in the component balances. $\mathbf{E_m}$ and $\mathbf{E_c}$ are given by Equations A-4 and A-5 respectively.

$$\mathbf{E_m} = \begin{bmatrix} -1 & 1 & 1 & 1 & 1 & 1 & 1 & 0 \\ -2 & 1 & 3 & 1.5 & 2.67 & 1.5 & 0 & 0 \\ -1 & 1 & 0.5 & 1.25 & 1 & 1 & 2 & -2 \end{bmatrix} \quad \text{(A-4)}$$

$$\mathbf{E_c} = \begin{bmatrix} 0 \\ 2 \\ 1 \end{bmatrix} \quad \text{(A-5)}$$

Once $\mathbf{E_m}$ and $\mathbf{E_c}$ have been determined, the redundancy matrix, $\mathbf{R}$, can be calculated. The rank of $\mathbf{R}$ should correspond to the number by which the system is overspecified; in this case the number is two. The reduced redundancy matrix, $\mathbf{R_r}$, is simply $\mathbf{R}$ with only the independent rows of $\mathbf{R}$ and will be used in further calculations. $\mathbf{R}$ and $\mathbf{R_r}$ are given by Equations A-6 and A-7 respectively.

$$\mathbf{R} = \mathbf{E_m} - \mathbf{E_c}\left(\mathbf{E_c}^{\mathrm{T}}\mathbf{E_c}\right)^{-1}\mathbf{E_c}^{\mathrm{T}}\mathbf{E_m} \quad \text{(A-6)}$$

$$\mathbf{R} = \begin{bmatrix} -1 & 1 & 1 & 1 & 1 & 1 & 1 & 0 \\ 0 & -0.2 & 0.4 & -0.2 & 0.1333 & -0.1 & -0.8 & 0.8 \\ 0 & 0.4 & -0.8 & 0.4 & -0.2667 & 0.2 & 1.6 & -1.6 \end{bmatrix}$$

$$\mathbf{R_r} = \begin{bmatrix} -1 & 1 & 1 & 1 & 1 & 1 & 1 & 0 \\ 0 & -0.2 & 0.4 & -0.2 & 0.1333 & -0.1 & -0.8 & 0.8 \end{bmatrix} \quad \text{(A-7)}$$

Since $\mathbf{E_m}$, $\mathbf{E_c}$ and $\mathbf{R}$ are only dependent on the component balances, they remain identical for each data point. The column vector, $\mathbf{q_m}$, contains all the measured values for this data point (in units of cmol.L^{-1}) and is given by Equation A-8.

$$\boldsymbol{q_m} = \begin{bmatrix} V_1 \\ V_2 \\ V_3 \\ V_4 \\ V_5 \\ V_6 \\ V_7 \\ V_8 \end{bmatrix} = \begin{bmatrix} 3.03 \\ 1.24 \\ 0.44 \\ 0.05 \\ 0.13 \\ 0.04 \\ 0.33 \\ 0.67 \end{bmatrix} \quad \text{(A-8)}$$

The variance-covariance matrix, **F**, is calculated by using an estimate of the expected errors as discussed in Section 2.5. It is assumed that the errors are all independent of each other and therefore only the diagonal elements of **F** are used. **F** is given by Equation A-9.

$$\mathbf{F} = \begin{bmatrix} (0.0031 + (0.02 \times 3.03))^2 & 0 & 0 & 0 & 0 & 0 & 0 & 0 \\ 0 & (0.0031 + (0.02 \times 1.24))^2 & 0 & 0 & 0 & 0 & 0 & 0 \\ 0 & 0 & (0.0031 + (0.07 \times 0.44))^2 & 0 & 0 & 0 & 0 & 0 \\ 0 & 0 & 0 & (0.0031 + (0.02 \times 0.05))^2 & 0 & 0 & 0 & 0 \\ 0 & 0 & 0 & 0 & (0.0031 + (0.02 \times 0.13))^2 & 0 & 0 & 0 \\ 0 & 0 & 0 & 0 & 0 & (0.0031 + (0.02 \times 0.04))^2 & 0 & 0 \\ 0 & 0 & 0 & 0 & 0 & 0 & (0.1 \times 0.33)^2 & 0 \\ 0 & 0 & 0 & 0 & 0 & 0 & 0 & (0.1 \times 0.67)^2 \end{bmatrix} \quad \text{(A-9)}$$

$$\mathbf{F} = 10^{-5} \begin{bmatrix} 410 & 0 & 0 & 0 & 0 & 0 & 0 & 0 \\ 0 & 78 & 0 & 0 & 0 & 0 & 0 & 0 \\ 0 & 0 & 120 & 0 & 0 & 0 & 0 & 0 \\ 0 & 0 & 0 & 1.8 & 0 & 0 & 0 & 0 \\ 0 & 0 & 0 & 0 & 3.4 & 0 & 0 & 0 \\ 0 & 0 & 0 & 0 & 0 & 1.7 & 0 & 0 \\ 0 & 0 & 0 & 0 & 0 & 0 & 110 & 0 \\ 0 & 0 & 0 & 0 & 0 & 0 & 0 & 440 \end{bmatrix}$$

The minimum variance estimate of the error vector, **δ**, is obtained by the minimisation problem in Equation A-10 [18].

$$Min_{\boldsymbol{\delta}} \left(\boldsymbol{\delta}^{\mathrm{T}} \mathbf{F}^{-1} \boldsymbol{\delta}\right) \quad \text{(A-10)}$$

The best estimate for solving the minimisation problem is given by Equation A-11 [18].

$$\boldsymbol{\delta}_{\mathbf{est.}} = \mathbf{F}\mathbf{R}_{\mathbf{r}}^{\mathrm{T}} \left(\mathbf{R}_{\mathbf{r}}\mathbf{F}\mathbf{R}_{\mathbf{r}}^{\mathrm{T}}\right)^{-1} \mathbf{R}_{\mathbf{r}}\mathbf{q}_{\mathbf{m}} \quad \text{(A-11)}$$

$$\boldsymbol{\delta}_{\mathbf{est.}} = \begin{bmatrix} 0.428 \\ -0.088 \\ -0.107 \\ 0.002 \\ -0.003 \\ 0.002 \\ -0.150 \\ 0.128 \end{bmatrix}$$

Finally, the reconciled measured values (in units of cmol.L^{-1}) are given by Equation A-12.

$$\mathbf{q}_{\mathbf{mreconciled}} = \mathbf{q}_{\mathbf{m}} - \boldsymbol{\delta}_{\mathbf{est.}} \quad \text{(A-12)}$$

$$\mathbf{q}_{\mathbf{mreconciled}} = \begin{bmatrix} 2.60 \\ 1.33 \\ 0.55 \\ 0.06 \\ 0.13 \\ 0.05 \\ 0.48 \\ 0.54 \end{bmatrix}$$

Table B-1 Raw data for HPLC and off-gas analyses

Time (h)	Glucose consumed ($g.L^{-1}$)	Fumaric acid produced ($g.L^{-1}$)	Ethanol produced ($g.L^{-1}$)	Malic acid produced ($g.L^{-1}$)	Glycerol produced ($g.L^{-1}$)	Succinic acid produced ($g.L^{-1}$)	CO_2 produced ($g.L^{-1}$)	O_2 consumed ($g.L^{-1}$)
Run 1 (pH 4, DO 60%)								
0	0.0	0.0	0.0	0.0	0.0	0.0	0.0	0.0
11	5.1	0.2	2.2	0.0	0.3	0.4	1.7	0.8
16	13.3	3.2	4.7	0.0	0.9	0.5	3.7	1.8
22	25.5	8.4	6.8	0.0	1.4	0.7	5.4	2.9
33	40.2	15.8	9.2	1.7	2.3	0.9	7.7	5.0
40	49.2	18.8	9.8	1.8	2.7	0.9	8.9	6.3
46	55.3	21.8	10.2	1.9	3.2	0.9	9.9	7.5
57	64.1	25.4	10.9	2.0	3.7	1.0	11.6	9.2
64	69.6	26.8	10.7	2.0	3.9	1.1	12.6	10.3
80	78.3	31.0	11.1	2.2	4.7	1.2	14.9	12.6
88	81.9	31.6	11.0	2.1	4.9	1.3	15.7	13.5
102	86.1	33.3	10.9	2.1	5.3	1.3	17.1	15.0
Run 2 (pH 5, DO 60%)								
0	0.0	0.0	0.0	0.0	0.0	0.0	0.0	0.0
6	1.9	0.0	0.5	0.0	0.0	0.4	0.0	1.5
18	14.3	3.3	5.2	0.0	0.7	0.5	4.5	5.8
23	25.6	7.5	7.5	0.0	1.1	0.6	6.1	7.1
32	40.7	14.0	9.9	0.0	1.8	0.8	8.3	9.4
43	56.1	20.2	11.4	1.6	2.4	1.0	10.2	11.9
47	61.5	21.8	11.5	1.6	2.5	0.9	10.8	12.8
56	70.2	25.9	12.1	1.6	3.0	1.2	12.2	15.1
65	79.0	29.8	12.1	1.9	3.4	0.9	13.3	17.1
71	83.5	31.7	11.8	1.9	3.6	0.9	13.9	18.2
80	88.7	33.9	11.1	1.9	4.0	1.2	14.6	20.0
91	90.8	35.9	10.2	1.8	4.0	1.4	14.7	21.3
Run 3 (pH 5, DO 80%)								
0	0.0	0.0	0.0	0.0	0.0	0.0	0.0	0.0
11	0.8	0.0	0.4	0.0	0.0	0.4	0.0	0.1
29	13.5	5.3	5.6	0.0	0.9	0.6	3.6	2.0
45	30.2	12.9	8.7	0.0	1.6	0.8	5.8	3.8
52	40.8	15.9	9.2	0.0	1.8	0.9	6.6	4.6
68	54.3	22.3	10.4	0.0	2.5	1.0	8.2	6.2
76	61.5	24.8	11.0	2.2	2.9	1.1	8.9	7.0
92	71.9	29.9	11.3	2.3	3.5	1.2	10.2	8.9
103	78.3	33.6	9.5	2.5	4.3	1.3	11.0	10.2
117	85.6	36.8	10.7	2.5	4.8	1.4	11.9	12.0
124	89.0	37.8	10.1	2.5	5.1	1.5	12.3	12.8
Run 4 (pH 5, DO 20%)								
0	0.0	0.0	0.0	0.0	0.0	0.0	0.0	0.0
12	4.8	0.3	3.3	0.0	0.3	0.4	1.7	0.2
21	19.4	5.3	7.9	0.0	1.0	0.6	4.9	1.0
34	36.8	11.1	11.7	0.0	1.5	0.8	7.8	1.8
45	49.3	15.1	13.8	0.0	1.9	0.9	10.0	2.6
59	60.9	19.7	15.8	1.8	2.2	1.0	12.1	3.2
72	70.8	23.3	17.6	1.9	2.5	1.1	14.2	3.9
105	88.8	28.8	20.0	1.9	3.0	1.2	18.6	5.1
118	91.2	30.0	18.9	1.6	3.1	1.2	19.5	5.5

Table B-2 Reconciled data for off−gas and HPLC analyses

Time (h)	Glucose consumed ($g.L^{-1}$)	Fumaric acid produced ($g.L^{-1}$)	Ethanol produced ($g.L^{-1}$)	Malic acid produced ($g.L^{-1}$)	Glycerol produced ($g.L^{-1}$)	Succinic acid produced ($g.L^{-1}$)	CO_2 produced ($g.L^{-1}$)	O_2 consumed ($g.L^{-1}$)
Run 1 (pH 4, DO 60%)								
0	0.0	0.0	0.0	0.0	0.0	0.0	0.0	0.0
11	1.6	0.3	0.2	0.3	0.0	0.7	0.0	0.1
16	14.2	3.4	4.1	0.0	0.7	0.5	6.1	2.4
22	24.7	7.8	6.9	0.0	1.1	0.6	8.7	3.5
33	38.7	14.5	10.0	0.0	1.8	0.9	11.7	5.3
40	52.4	21.1	12.3	1.7	2.4	1.1	14.2	7.6
46	56.2	22.8	13.1	1.7	2.6	0.9	15.5	8.4
57	63.9	27.2	14.0	1.7	3.0	1.2	17.3	10.3
64	70.4	31.5	14.5	1.9	3.4	0.9	19.0	12.3
80	73.5	33.6	14.4	2.0	3.7	0.9	20.0	13.6
88	76.8	36.2	13.8	2.0	4.0	1.2	21.2	15.6
102	78.0	38.4	12.7	1.9	4.1	1.5	21.3	17.1
Run 2 (pH 5, DO 60%)								
0	0.0	0.0	0.0	0.0	0.0	0.0	0.0	0.0
6	4.9	0.3	1.7	0.1	0.3	0.5	2.3	0.6
18	13.2	3.3	3.9	0.0	0.9	0.6	4.7	1.5
23	24.6	8.6	6.7	0.0	1.5	0.7	6.9	2.5
32	39.4	16.1	9.2	1.7	2.3	0.9	8.9	4.5
43	46.8	19.4	10.8	1.8	2.8	0.9	10.8	5.7
47	52.3	22.5	11.5	1.9	3.2	1.0	12.0	6.9
56	59.9	26.3	12.6	2.0	3.7	1.1	14.2	8.7
65	63.6	27.9	13.0	2.0	4.0	1.1	15.9	10.1
71	71.5	32.3	13.5	2.2	4.8	1.3	18.4	12.7
80	73.7	33.1	13.6	2.2	5.1	1.3	19.9	13.9
91	77.1	34.8	13.5	2.2	5.4	1.3	21.8	15.7
Run 3 (pH 5, DO 80%)								
0	0.0	0.0	0.0	0.0	0.0	0.0	0.0	0.0
11	0.8	0.1	0.1	0.2	0.0	0.5	0.0	0.1
29	14.0	5.2	3.5	0.0	0.8	0.6	3.9	1.7
45	30.2	13.1	7.4	0.0	1.6	0.8	6.8	3.2
52	38.6	16.6	9.8	0.0	1.9	0.9	8.6	3.8
68	50.4	23.4	11.9	0.0	2.5	1.1	10.5	5.4
76	56.9	25.9	12.7	2.2	2.9	1.1	11.0	6.4
92	65.6	31.3	13.6	2.4	3.6	1.3	12.5	8.3
103	69.3	35.5	12.0	2.5	4.4	1.4	13.1	10.9
117	76.1	38.9	13.2	2.6	4.9	1.5	14.6	12.0
124	77.6	40.1	12.8	2.5	5.2	1.5	15.4	13.2
Run 4 (pH 5, DO 20%)								
0	0.0	0.0	0.0	0.0	0.0	0.0	0.0	0.0
12	4.9	0.3	2.0	0.0	0.2	0.4	2.0	0.2
21	19.5	5.3	6.5	0.0	1.0	0.6	5.8	1.0
34	35.8	11.3	11.7	0.0	1.5	0.8	9.6	1.7
45	47.1	15.4	15.2	0.0	1.9	0.9	12.4	2.5
59	58.6	20.1	18.0	1.9	2.3	1.0	13.9	3.2
72	67.7	23.7	20.6	1.9	2.5	1.1	16.0	3.9
105	83.5	29.5	25.4	1.9	3.0	1.2	20.4	5.3
118	84.6	30.7	25.2	1.6	3.1	1.3	20.7	5.9

References

[1] T. Werpy, G. Petersen, A. Aden, J. Bozell, J. Holladay, J. White, A. Manheim, D. Eliot, L. Lasure, S. Jones, Top Value Added Chemicals From Biomass. Volume 1-Results of Screening for Potential Candidates From Sugars and Synthesis Gas, DTIC Document, 2004.

[2] J.J. Beauprez, M. De Mey, W.K. Soetaert, Microbial succinic acid production: Natural versus metabolic engineered producers, Process Biochem. 45 (2010) 1103–1114.

[3] Grand View Research, Maleic Anhydride Market Analysis By Application (Unsaturated Polyster Resins, BDO, Additives, Copolymers) and Segment Forecasts To 2020, 2014.

[4] C.A. Roa Engel, A.J.J. Straathof, T.W. Zijlmans, W.M. van Gulik, L. a M. van der Wielen, Fumaric acid production by fermentation., Appl. Microbiol. Biotechnol. 78 (2008) 379–89.

[5] Q. Xu, S. Li, H. Huang, J. Wen, Key technologies for the industrial production of fumaric acid by fermentation., Biotechnol. Adv. 30 (2012) 1685–96.

[6] Y.-S. Jang, B. Kim, J.H. Shin, Y.J. Choi, S. Choi, C.W. Song, J. Lee, H.G. Park, S.Y. Lee, Bio-based production of C2-C6 platform chemicals., Biotechnol. Bioeng. 109 (2012) 2437–59.

[7] G. Xu, X. Chen, L. Liu, L. Jiang, Fumaric acid production in Saccharomyces cerevisiae by simultaneous use of oxidative and reductive routes., Bioresour. Technol. 148 (2013) 91–6.

[8] X. Chen, J. Wu, W. Song, L. Zhang, H. Wang, L. Liu, Fumaric Acid Production by Torulopsis glabrata: Engineering the Urea Cycle and the Purine Nucleotide Cycle., Biotechnol. Bioeng. 112 (2014) 156–167.

[9] J. Du, N. Cao, C.S. Gong, G.T. Tsao, N. Yuan, Fumaric acid production in airlift loop reactor with porous sparger., Appl. Biochem. Biotechnol. 63-65 (1997) 541–56.

[10] N. Cao, J. Du, C. Chen, C.S. Gong, G.T. Tsao, Production of fumaric acid by immobilized rhizopus using rotary biofilm contactor., Appl. Biochem. Biotechnol. 63-65 (1997) 387–94.

[11] Y. Zhou, J. Du, G.T. Tsao, Comparison of fumaric acid production by Rhizopus oryzae using different neutralizing agents., Bioprocess Biosyst. Eng. 25 (2002) 179–81.

[12] C.A. Roa Engel, W.M. van Gulik, L. Marang, L. a M. van der Wielen, A.J.J. Straathof, Development of a low pH fermentation strategy for fumaric acid production by Rhizopus oryzae., Enzyme Microb. Technol. 48 (2011) 39–47.

[13] Y. Zhou, J. Du, G.T. Tsao, Mycelial pellet formation by Rhizopus oryzae ATCC 20344., Appl. Biochem. Biotechnol. 84-86 (2000) 779–89.

[14] Y. Fu, Q. Xu, S. Li, Y. Chen, H. Huang, Strain improvement of Rhizopus oryzae for over-production of fumaric acid by reducing ethanol synthesis pathway, Korean J. Chem. …. 27 (2010) 183–186.

[15] D.-M. Bai, M.-Z. Jia, X.-M. Zhao, R. Ban, F. Shen, X.-G. Li, S.-M. Xu, -lactic acid production by pellet-form Rhizopus oryzae R1021 in a stirred tank fermentor, Chem. Eng. Sci. 58 (2003) 785–791.

[16] I. Goldberg, J.S. Rokem, O. Pines, Organic acids: Old metabolites, new themes, J. Chem. Technol. Biotechnol. 81 (2006) 1601–1611.

[17] J. Villadsen, J. Nielsen, G. Lidén, Bioreaction Engineering Principles, Springer US,

Boston, MA, 2011.

[18] N.S. Wang, G. Stephanopoulos, Application of macroscopic balances to the identification of gross measurement errors, Biotechnol. Bioeng. 25 (1983) 2177–2208.

[19] Y. Ding, S. Li, C. Dou, Y. Yu, H. Huang, Production of fumaric acid by Rhizopus oryzae: role of carbon-nitrogen ratio., Appl. Biochem. Biotechnol. 164 (2011) 1461–7.

[20] Y. Fu, Q. Xu, S. Li, H. Huang, Y. Chen, A novel multi-stage preculture strategy of Rhizopus oryzae ME-F12 for fumaric acid production in a stirred-tank reactor, World J. Microbiol. Biotechnol. 25 (2009) 1871–1876.

[21] R. A Rhodes, A A Lagoda, T.J. Misenheimer, M.L. Smith, R.F. Anderson, R.W. Jackson, Production of Fumaric Acid in 20-Liter Fermentors., Appl. Microbiol. 10 (1962) 9–15.

[22] P. Song, S. Li, Y. Ding, Q. Xu, H. Huang, Expression and characterization of fumarase (FUMR) from Rhizopus oryzae., Fungal Biol. 115 (2011) 49–53.

[23] E. Riscaldati, M. Moresi, Ammonium fumarate production by free or immobilised Rhizopus arrhizus in bench and laboratory-scale bioreactors, J. Chem. …. 77 (2002) 1013–1024.

[24] Y. Q. Fu, S. Li, Y. Chen, Q. Xu, H. Huang, X.-Y. Sheng, Enhancement of fumaric acid production by Rhizopus oryzae using a two-stage dissolved oxygen control strategy., Appl. Biochem. Biotechnol. 162 (2010) 1031–8.